



# Structural, electrical, and electrochemical properties of poly(vinylidene fluoride-co-hexafluoropropylene)/poly(vinyl acetate)-based polymer blend electrolytes for rechargeable magnesium ion batteries

S. Ponmani<sup>1</sup> · J. Kalaiselvi<sup>1</sup> · M. Ramesh Prabhu<sup>1</sup>

Received: 25 January 2018 / Revised: 13 April 2018 / Accepted: 16 April 2018 / Published online: 3 May 2018  
© Springer-Verlag GmbH Germany, part of Springer Nature 2018

## Abstract

An attempt has been made to prepare a new blend polymer electrolytes (BPEs) based on PVdF-co-HFP and PVAc doped with Mg (ClO<sub>4</sub>)<sub>2</sub> by using the solvent-casting technique. The physicochemical properties of the as prepared polymer electrolytes were characterized by XRD, FTIR, SEM, TG/DTA, linear sweep voltammetry (LSV), and cyclic voltammetry (CV). The maximum ionic conductivity value  $3.85 \times 10^{-5} \text{ S cm}^{-1}$  has been observed for PVdF-co-HFP (69)-PVAc (23)-Mg (ClO<sub>4</sub>)<sub>2</sub> (8 wt%) system at 30 °C using AC impedance spectroscopic technique. The FTIR analysis confirms the complex formation between the polymers and salts. The TG/DTA studies showed the thermal stability of the film. The polymer electrolyte membrane shows a wide electrochemical stability window, and the temperature dependence of ionic conductivity obeys the Arrhenius rule.

**Keywords** Blend polymer electrolytes · Cyclic voltammetry · Electrochemical stability · Mg (ClO<sub>4</sub>)<sub>2</sub> · SEM

## Abbreviations

PVdF-HFP	poly(vinylidene fluoride-co-hexafluoropropylene)
PVAc	poly(vinyl acetate)
XRD	X-ray diffraction,
FTIR	Fourier-transform infrared spectroscopy
SEM	scanning electron microscope,
TG/DTA	Thermogravimetric/differential thermal analysis
PMMA	poly(methyl methacrylate)
PEG	polyethylene glycol

## Introduction

In recent years, environmental pollution and power crisis have been severely accumulated due to the extreme utilization of

fossil fuel resources. To defeat these problems, clear energy resources and related energy conversion and storage materials and devices are highly demanded [1]. Electrical energy storage technologies play an important role in the demand for green and sustainable energy. Rechargeable batteries or secondary batteries, such as Li-ion batteries, Na-ion batteries, and Mg-ion batteries, reversibly convert between electrical and chemical energy via redox reaction, thus storing the energy as chemical potential in their electrodes. [2].

The polymer battery has the advantage of having a higher energy density, solvent-free condition easy process ability, and being leakage proof and light in weight. The interest on solid polymer electrolytes has grown during the last decades together with the search of new and more efficient, high performance devices for energy conversion and storages [3]. Rechargeable lithium metal batteries with high specific capacities are still commercially unavailable. Even though the Li ion battery has the choice in the view of its specific capacity and cycle stability. However, the application of LIBs in electric vehicles (EVs) or renewable energy storage is largely limited due to the finite energy/power density [4]. The lithium ion-conducting gel polymer electrolytes has safety problems, limitations, and relatively expensive, because they are highly reactive in nature and also toxic. Apart from lithium batteries, certain magnesium, zinc, and sodium batteries are reported [5–7]. So, to a greater extent, researchers focus on developing

**Electronic supplementary material** The online version of this article (<https://doi.org/10.1007/s10008-018-3971-6>) contains supplementary material, which is available to authorized users.

✉ M. Ramesh Prabhu  
mkram83@gmail.com

<sup>1</sup> Department of Physics, Alagappa University, Karaikudi 630 004, India

solid state  $\text{Mg}^{2+}$  ion-conducting electrolytes to achieve rechargeability [8–10].

Magnesium possesses a many number of characteristics that make it attractive electrode material for rechargeable batteries, including its low cost, relative abundance (fifth most abundant materials on earth), high safety, ease of handling, and its low toxicity which allows for urban waste disposal [11]. In future, the rechargeable magnesium batteries have a wide scope in the future in the analysis of negligible hazards and enhanced safety [12, 13]. There have been some studies on the solid polymer electrolytes based on magnesium salts [14–18]. Polymer blending can avoid problems associated with a low ionic conductivity of the system with property that could not be obtained with the use of a single polymer [19]. The blending of the polymers is one of the effective methods to improve the mechanical stability and electrical conductivity of the polymeric materials. Many researchers have reported on the blend polymer electrolyte (BPE) system, such as PVdF-HFP/PMMA, PVdF-HFP/PVAc, PVAc/PMMA, PVdF-HFP/PVAc, PVdF-HFP/PEG, and PVAc/PVdF-HFP [20–25] with different lithium salts and ammonium salts, respectively. The review of the literature reveals that attention has been given to the polymer electrolytes based on PVdF-HFP and PVAc BPE for  $\text{Mg}^{2+}$  ion battery.

Various methods have been adopted to reduce crystallinity of polymer electrolytes and to increase segmental mobility of the host polymer, such as blending [26, 27], copolymerization [28–31], cross linking, and plasticization of polymer matrix [32–35]. Among the polymer electrolytes, the PVdF-HFP-based gel polymer films have received much attention since they have both crystalline VdF and amorphous HFP units. The amorphous phase is capable of trapping large amount of electrolyte, facilitating ion migration, while the crystalline phase provides a structural integrity to support a free standing film formation. In addition, the PVdF-HFP-based gel polymer electrolyte films are mechanically stiff and strong, thermally, and chemically stable [36–39]. The PVAc happens to be one of the polymers which possess a large dipole moment and high relaxation time which are due to its side chains connected to ester groups in the side chain [40, 41]. PVAc is a proper contender to achieve high ionic conductivity at ambient temperature, mechanical stability, and comfortable film formation among the various choices. To improve the ionic conductivity, an attempt has been made to identify the effects of  $\text{Mg}(\text{ClO}_4)_2$  on the new PVdF-co-HFP/PVAc-based BPEs.

## Materials and instrumentations

Poly(vinylidene fluoride-co-hexafluoropropylene) (PVdF-HFP) with an average molecular weight of ( $M_w$ )  $\sim 400,000$  and polyvinyl acetate (PVAc) and magnesium perchlorate

$\text{Mg}(\text{ClO}_4)_2$  salt were obtained from Sigma-Aldrich. All the composite polymer electrolytes were prepared by using a solvent-casting technique. They were dried under vacuum at  $80^\circ\text{C}$  at about 10 h for removing the moisture or impurities. The polymers and the salts were first dissolved in tetrahydrofuran (THF) separately and then mixed together. The complex mixture was stirred continuously about 24 h to ensure the fine and homogeneous mixture. The acquired homogeneous solution was poured into the Petri dish to allow the Petri dish to vacuum oven to evaporate the residual solvent from the complex at  $60^\circ\text{C}$  for 5 h. The obtained composite polymer electrolytes were stored in a vacuum desiccator for further studies. The prepared BPE with flexible and free standing film is shown in Fig. 1.

The structural analysis of the prepared polymer composites was analyzed by XRD using an X'pert PRO PANalytical X-ray diffractometer. The complex formation between the polymer and salt was confirmed by FTIR using SPECTRA RXI, Perkin Elmer spectrophotometer in the range of  $400\text{--}4000\text{ cm}^{-1}$ . Thermal stability of the polymer electrolyte was carried out by thermogravimetric/differential thermal analysis (TG/DTA) using SIINT 6300, Japan, with the heating rate of  $10^\circ\text{C min}^{-1}$  under the nitrogen atmosphere from room temperature to  $800^\circ\text{C}$ . The morphology of the polymer electrolytes was examined by gold sputter-coated scanning electron microscopy (SEM) (FEI Quanta 250 Microscope, Netherlands). Conductivity studies were carried out with the help of stainless steel (SS)-blocking electrodes using a computer-controlled microauto lab type III Potentiostat/Galvanostat in the frequency range of 10 Hz to 100 MHz over the temperature range of  $30\text{--}90^\circ\text{C}$ , and the electrochemical stability of the maximum



Fig. 1 The flexible and free standing BPE

conducting electrolyte was evaluated by means of linear sweep voltammetry (LSV) using SS as the working electrode and reference electrode. The high conducting polymer electrolytes (Q2) from the prepared BPEs has been constructed, and their results are discussed. The composition of the prepared polymer electrolytes is shown in Table 1.

## Results and discussion

### XRD

The XRD patterns of the PVdF-HFP, PVAc,  $\text{Mg}(\text{ClO}_4)_2$  of the pure polymer, salt, and composite gel polymer electrolytes are shown in Fig. 2. The pure PVdF-HFP shows the semi-crystalline microstructure, i.e., the coexistence of mixed crystalline and amorphous nature of the material with predominant peaks at  $2\theta = 17^\circ$ ,  $20^\circ$ , and  $38^\circ$  [17]. The PVAc shows the broad hump and which confirm the amorphous nature of the polymer [42]. The diffraction pattern of the  $(\text{MgClO}_4)_2$  salt showed a high intense peak, which revealed the crystalline nature of the salts and also well matched with the JCPDS (No: 37-0523). The  $\text{Mg}(\text{ClO}_4)_2$  crystalline peaks are absent in the polymer composite electrolytes. The diffractogram of a polymer electrolyte shows a broadened peak between  $10^\circ$  and  $25^\circ$ . The PVdF-HFP peak is masked at  $20^\circ$ ; the broad peak and the intensity of the peak decreased. These changes reveal that the gel polymer electrolyte is predominantly amorphous and its crystallinity is depressed due to the immobilization of liquid electrolyte in PVdF-HFP. This inciates that the liquid electrolyte solution most likely blends with the PVdF-HFP at the molecular level. This confirms that the interaction takes place between the constituents that are involved in the preparation of the composite electrolytes. The sample Q2 is more amorphous compared to other polymer composites. The amorphous nature which could be the reason for high conductivity of the film Q2.

### FTIR analysis

FTIR transmittance spectra of pure and the prepared complexes are presented in Fig. 3. The spectrum of PVdF-HFP,

**Table 1** The composition of the prepared polymer electrolytes

PVdF-HFP (wt%)	PVAc (wt%)	$\text{Mg}(\text{ClO}_4)_2$ (wt%)	Sample code
92	0	8	Q1
69	23	8	Q2
46	46	8	Q3
23	69	8	Q4
0	92	8	Q5

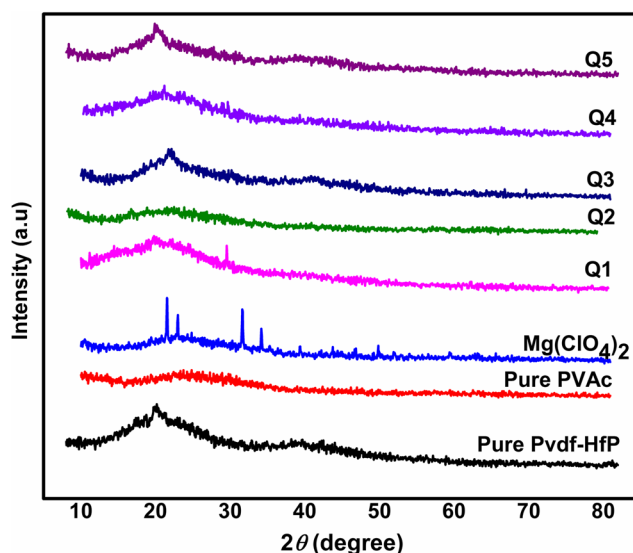


**Fig. 2** XRD pattern for pure and prepared polymer electrolytes

the crystalline phase of VdF unit identified by the vibration bands of  $981$ ,  $759$  and  $618\text{ cm}^{-1}$ , is due to a non-polar trans-gauche conformation (i.e.,  $\alpha$  phase) of the semi-crystalline PVdF-HFP [43–45]. The vibration band of PVdF-HFP has been observed at  $1400$  and  $1200\text{ cm}^{-1}$  for  $\text{—CF}$  and  $\text{—CF}_2$  groups. The peaks at  $527\text{ cm}^{-1}$  can be assigned to the bending vibrations of  $\text{—CF}_2$ . The bands at  $842$  and  $879\text{ cm}^{-1}$ , assigned to amorphous phase, appear as symmetrical stretching; vibration and the bands are shifted slightly in the polymer complexes, respectively. These observations indicate the substantial conformational changes in the crystalline texture of the host polymer PVdF-HFP due to the interaction with the PVAc and salt electrolytes. The disappearance of some bands associated with crystalline phase and the appearance of the

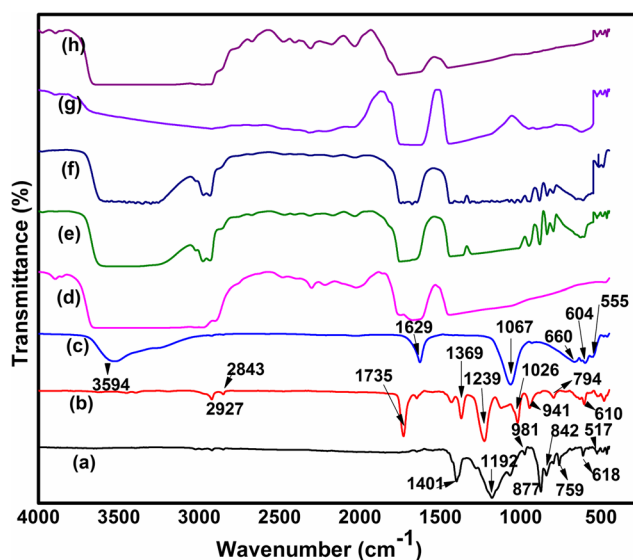


**Fig. 3** FTIR spectra of **a** pure PVdF-HFP, **b** pure PVAc, **c**  $\text{Mg}(\text{ClO}_4)_2$  salt, **d** Q1, **e** Q2, **f** Q3, **g** Q4, and **h** Q5 samples

bands of amorphous phase of the polymer indicate the reduction of crystallinity and dominance of the amorphous phase in the composite gel polymer electrolyte.

The vibration bands at 2928, 1735, 1026, 1369, and 1229  $\text{cm}^{-1}$  are attributed to  $\text{CH}_3$  asymmetric,  $\text{C}=\text{O}$  group,  $\text{C}-\text{O}$  stretching, and  $-\text{CH}_3$  symmetric bending modes of pure PVAc. The peaks at 947, 607, and 794  $\text{cm}^{-1}$  are ascribed to  $-\text{CH}$  bending and  $\text{CH}_3(\text{C}-\text{O})$  group, and the  $\text{C}-\text{H}$  rocking mode of vibration of PVAc has been confirmed [46, 47]. The stretching vibration mode of  $\text{ClO}_4^-$  anion observed in the range of 650–600  $\text{cm}^{-1}$  has been probed to get the information associated with the degree of salt dissociation in the composite gel polymer electrolyte [48, 49]. These peaks are shifted in Q1, Q2, Q3, Q4, and Q5. The changes in the frequency characteristics of the electrolyte membranes are given in Table 2 and confirm the complexation in the measured polymer electrolytes.

### TG/DTA analysis

Figure 4a–e shows the TG/DTA analysis of the prepared polymer composite electrolytes. It can be seen that from the TG curves, the initial weight loss occurs from 77 to 83  $^{\circ}\text{C}$  with a weight loss of 5, 3, 8, 4, and 9 wt% for all the samples due to the residual solvent and moisture at the time of loading the sample. It is observed that the second weight loss occurs at 245 to 274  $^{\circ}\text{C}$  for prepared samples, respectively, with the corresponding weight losses which are 17, 16, 19, 18, and 20 wt%. This may be due to the structural decomposition of the polymer blends. The complete decomposition of the sample takes place between 522 and 526  $^{\circ}\text{C}$  with the corresponding weight loss of about 78, 81, 73, 78, and 71 wt%. After nearly 650  $^{\circ}\text{C}$ , no appreciable weight loss is observed.

In DTA curve, the first exothermic peaks occurs in the range of 245 to 274  $^{\circ}\text{C}$ , and the second exothermic peaks occurs in the range of 523 to 528  $^{\circ}\text{C}$  in the prepared polymer electrolytes. This indicates the decomposition of the polymer film is in good agreement with the observed TG results.

### SEM

Figure 5a, b shows the SEM image with different magnifications of the maximum conducting BPE (Q2) film. In general, a porous structure is essential for ionic transport from one site to another site. Hence, large porosity and small pore size are fundamental for a good separator, when the surface shows enormous number of pores and hence higher ion migration. The uniformly dispersed pores in the polymer microstructure lead to the retention of liquid electrolyte and formation of their better connectivity through the polymer, giving rise to have possibility of high ionic conductivity. Here, the sample shows the large number of pores which is evident from the picture, and this leads to yield the high conductivity. This is well matched and confirmed from the impedance analysis and also from XRD.

### Impedance analysis

Figure 6 shows the Nyquist plot of the prepared polymer composite electrolytes at 30  $^{\circ}\text{C}$ . The ionic conductivity values of the electrolytes are calculated by using Eq. (1)

$$\sigma = l/R_b A \quad (1)$$

where  $l$  and  $A$  are the thickness and the area of the polymer electrolytes film, and  $R_b$  is the bulk resistance of the electrolyte film. The bulk resistance can be calculated from the

**Table 2** The FTIR assigned peaks for pure and the prepared polymer electrolytes, (Q1) PVdF-HFP (92)/PVAc(0)/ $\text{Mg}(\text{ClO}_4)_2$  (8), (Q2) PVdF-HFP (69)/PVAc(23)/ $\text{Mg}(\text{ClO}_4)_2$ (8), (Q3) PVdF-HFP (46)/PVAc(46)/ $\text{Mg}(\text{ClO}_4)_2$ (8), (Q4) PVdF-HFP (23)/PVAc(69)/ $\text{Mg}(\text{ClO}_4)_2$ (8), (Q5) PVdF-HFP (0)/PVAc(92)/ $\text{Mg}(\text{ClO}_4)_2$ (8)

Bands assignment	Wavenumber ( $\text{cm}^{-1}$ )						
	Pure PVdF-co-HFP	Pure PVAc	Q1	Q2	Q3	Q4	Q5
$-\text{CF}$ groups	1400	–	1406	1414	1402	1433	1398
Non-polar trans-gauche ( $\alpha$ phase)	981	–	–	979	975	983	–
Non-polar trans-gauche ( $\alpha$ phase)	759	–	765	762	758	769	759
Non-polar trans-gauche ( $\alpha$ phase)	618	–	625	608	615	610	624
$\text{CH}_3$ (asymmetric stretching)	–	2928	2920	2934	2928	2920	2934
$\text{CO}$ (stretching)	–	1735	1748	1748	1732	1743	1734
$\text{C}-\text{O}$ (stretching)	–	1026	–	1011	1021	1026	–
$-\text{CH}$ bending	–	941	–	947	947	941	–
$\text{ClO}_4^-$	–	610	618	613	615	620	612

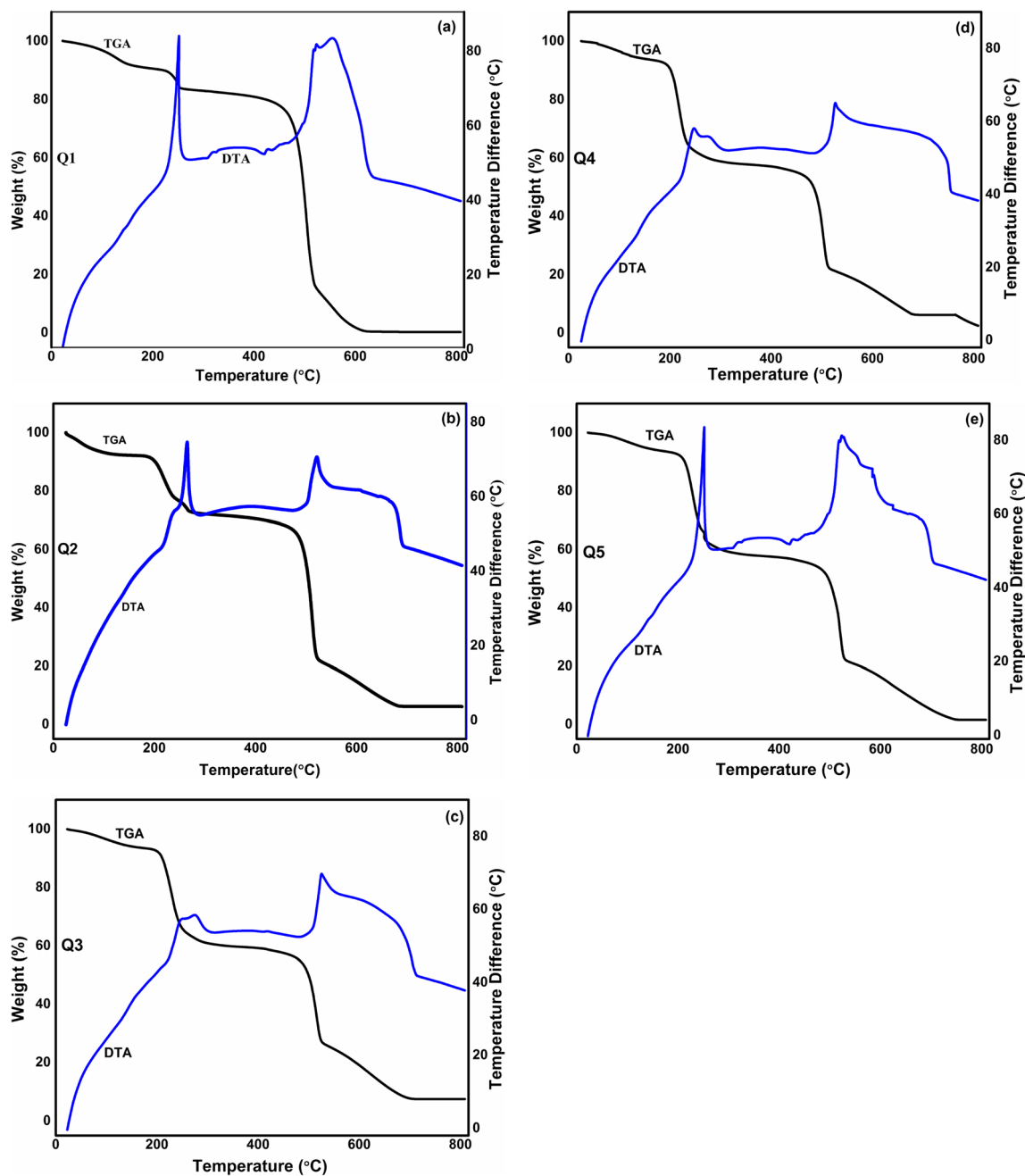


Fig. 4 TG/DTA analysis of the Q1, Q2, Q3, Q4, and Q5 samples

intercept of high-frequency or low-frequency spike or semi-circle on the  $Z'$  axis or  $X$  axis.

The impedance plot shows a high-frequency semi-circle for Q5 sample, and the other sample shows the spike at low-frequency range. The highest ionic conductivity at ambient temperature is found to be  $3.85 \times 10^{-5}$  S/cm for the Q2 sample. The semi-circular portions corresponding to the high-frequency region are absent (inset figure) except Q5. This indicates that the majority of the current carriers in the electrolyte medium are ions, and that the total conductivity is mainly due to the ion conduction [50].

### Temperature dependence of ionic conductivity

Figure 7 represents the temperature dependence conductivity for the prepared polymer electrolytes. The conductivity increases with increasing temperature for all the prepared polymer electrolytes, and it follows the Arrhenius type of thermally activated process given by the relation

$$\sigma = \sigma_0 \exp(-E_a/kT)$$

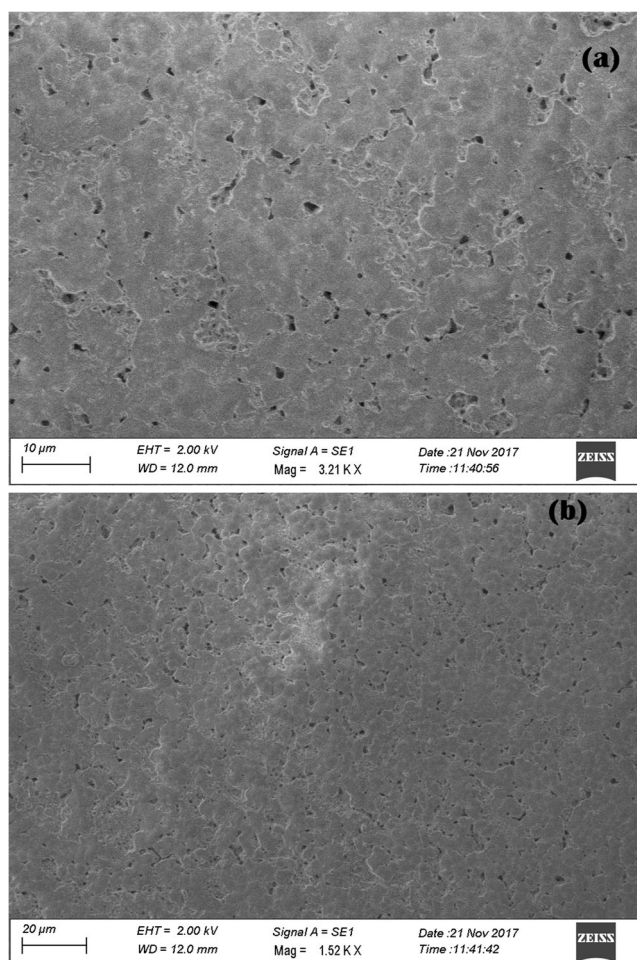


**Fig. 5** **a** and **b** SEM image of the sample (Q2) having maximum ionic conductivity. **a** 3.25 K. **b** 1.52 K

where  $\sigma_0$  is the pre-exponential factor,  $Ea$  is the activation energy in eV,  $k$  is the Boltzmann constant, and  $T$  is the absolute temperature. The activation energy  $Ea$  is the combination of

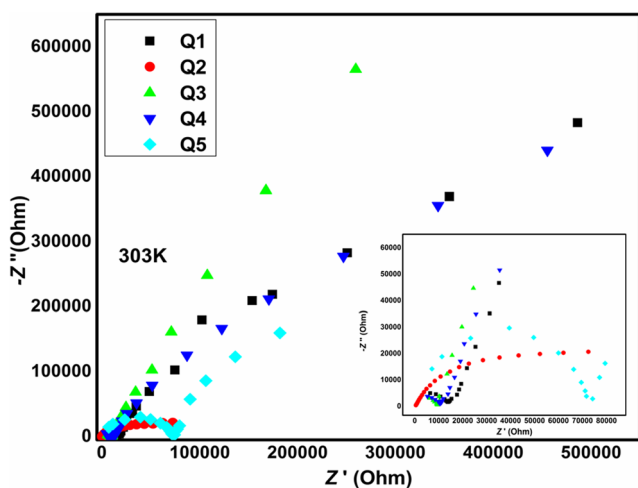


**Fig. 6** Room temperature of the complex impedance plot of the prepared samples

the energy of defect formation, and the energy of migration is calculated for all the prepared polymer electrolytes by using the Arrhenius plot. The low activation energy for the magnesium ion transport is due to the complete amorphous nature which provides a bigger free volume of the polymer electrolytes. As the amorphous region increases, the polymer chain acquires faster internal modes in which bond rotation produces segmental motion to favor the inter- and intra-chain ion hopping and thus, the conductivity becomes high [51, 52]. The sample Q2 has a higher ionic conductivity ( $6.27 \times 10^{-4}$  S/cm at 90 °C) and the lower activation energy (3.37 eV) compared to other compositions.

## Dielectric analysis

Figure 8a, b represents the frequency dependence of  $\epsilon'(\omega)$  and  $\epsilon''(\omega)$  of the prepared polymer electrolytes at room temperature (30 °C), respectively. From the obtained dielectric constant spectra, the values of the  $\epsilon'(\omega)$  are high at low frequency and become constant at high frequency. Similarly, the high dielectric loss is obtained at the low frequency, and it decreases when the frequency increases.

At low frequency side, the values of the dielectric constant and also dielectric loss are high; this may due to the free charge carriers have enough time to build up at the interfaces between the electrode and electrolytes, leading to the localization of charge carriers [53]. At low frequency, the high value of dielectric constant is obtained; this is due to the contribution of the electrode polarization effects.

At high frequency, the periodic reversal of the electric field occurs so fast that there is no excess ion diffusion in the direction of the applied field. The fluctuations of the charge carriers in the directions of the field now lag behind, which ensure the low dielectric values for increasing the frequency.

Generally, the spectrum consists of two relaxation process, such as  $\alpha$  and  $\beta$ . The  $\alpha$  relaxation process is taking place at low frequency. It means it is observably at high temperature, which may be caused by the movements of the main segments of the polymer. Then the  $\beta$  relaxation process takes place at high-frequency region. It means that it is obviously at low temperature, which may be caused due to the side group dipoles and the nearest part of the backbones. The obtained spectrum shows  $\alpha$  relaxation process. From the prepared BPEs, the high dielectric constant and dielectric loss are obtained for the sample Q2.

## Modulus spectra analysis

Figure 9a, b shows the modulus spectra of the prepared polymer electrolytes. The electric modulus is defined as

$$M^* = M' - iM''$$

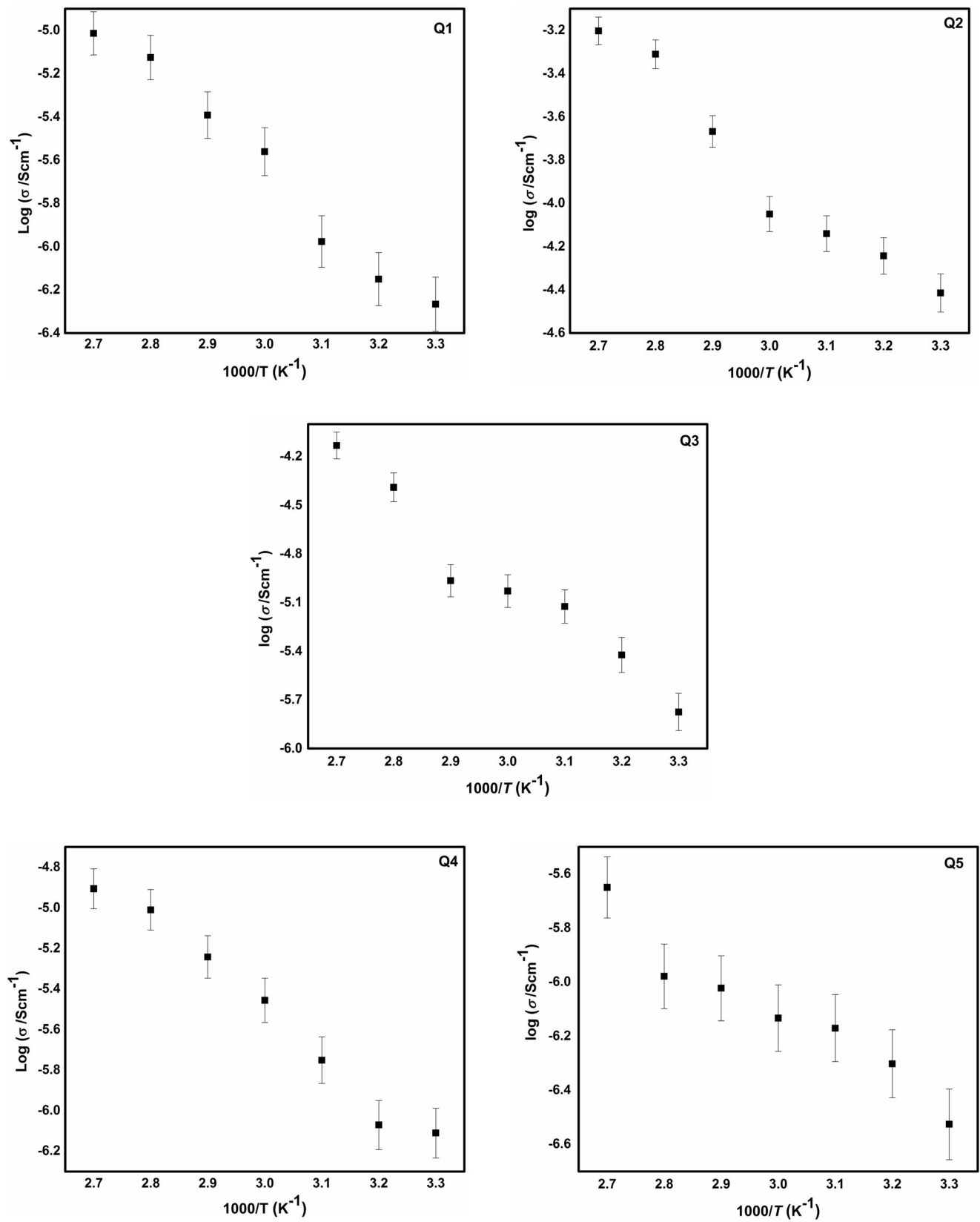
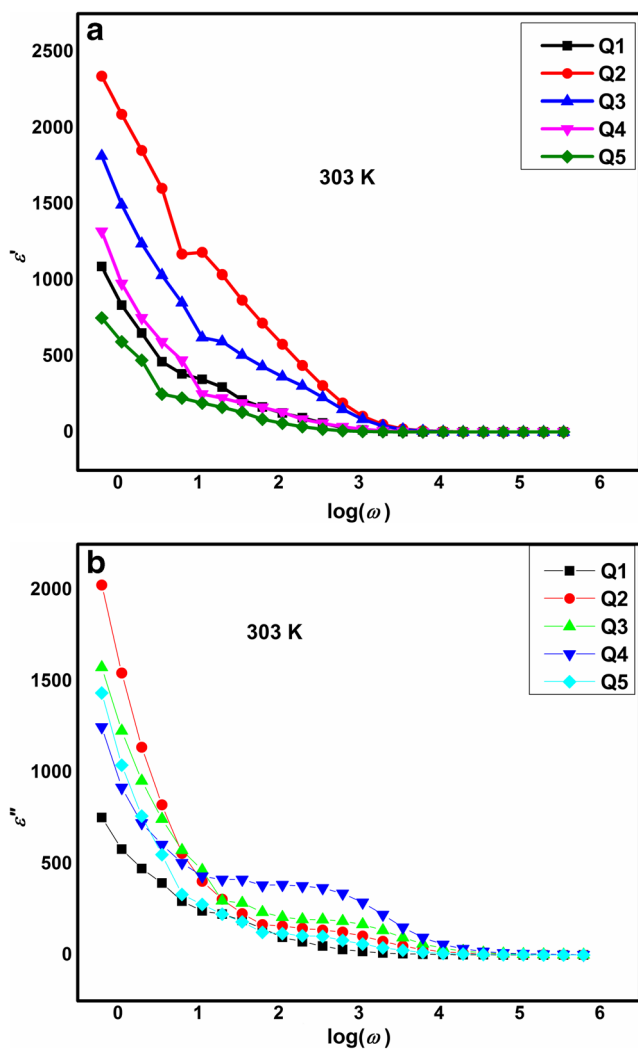


Fig. 7 Temperature-dependent ionic conductivity plot of the prepared samples



**Fig. 8** Room temperature frequency dependence of **a**  $\epsilon''(\omega)$  and **b**  $\epsilon''(\omega)$  for the prepared samples

where  $M'$  and  $M''$  are the real and imaginary parts of the polymer electrolytes. Both  $M'$  and  $M''$  are observed approximately zero at low frequency side that corresponds to the repression of the electrode polarization effect at the electrode-electrolyte interfaces. A long tail obtained for both the  $M'$  and  $M''$  modulus spectra at low frequency may be convincingly accredited as due to the large capacitance coupled with the electrode, and also due to the occurrence of the negligible electrode polarization contribution, the  $M'$  and  $M''$  decreases towards the low-frequency region.

Further increases of the frequency values of  $M'$  and  $M''$  also increase and reach the maximum value at higher frequency, which implies the distribution of relaxation process over a range of frequency. The  $M'$  and  $M''$  spectrum shows a perfect and distinct dispersion that demonstrate a distinctive increase in high frequency. The observed modulus spectrum for the prepared BPEs at high-frequency region that reveals the electrolytes has a good ionic conductivity. The spectrum at high-

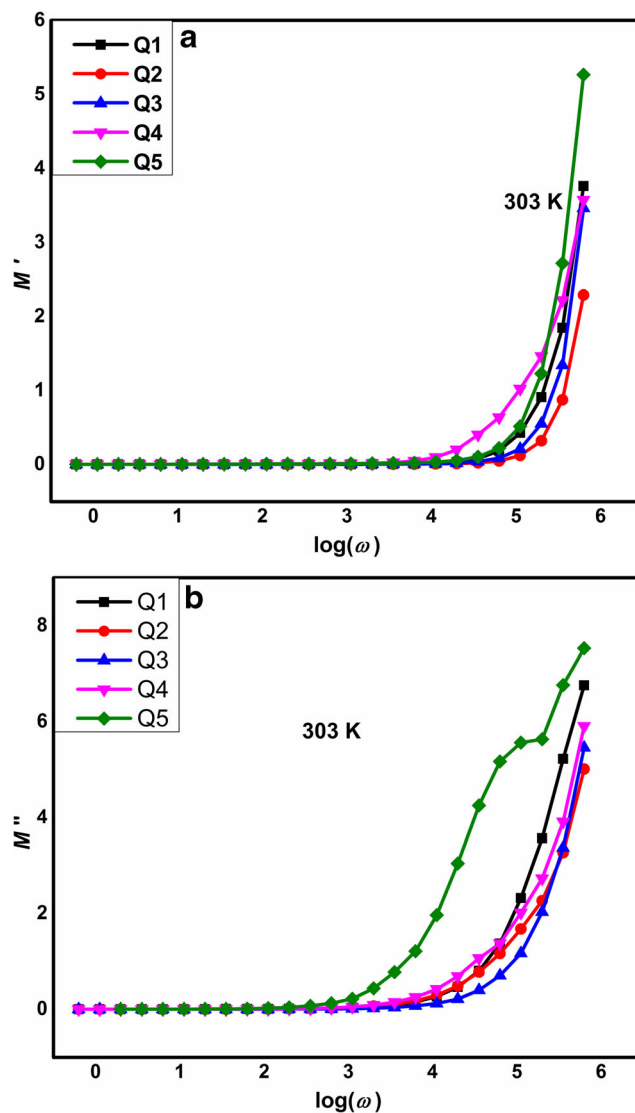


**Fig. 9** Room temperature frequency dependence of **a**  $M'(\omega)$  and **b**  $M''(\omega)$  for the prepared samples

frequency region may be due to the bulk effect. The sharp increase in the high-frequency region, which indicates the possibility of the ionic conduction, takes place and contained by these polymer blend electrolytes. The maximum peak shift towards the high frequency for the optimum blend ratio of Q2 sample implies that it has small relaxation time.

### Loss tangent spectra

Figure 10 shows the dielectric relaxation parameter of the polymer electrolyte from the variation of  $\tan\delta$  with frequency for the prepared polymer electrolytes at 30 °C. The dielectric loss tangent ( $\tan\delta$ ) can be defined by the equation

$$\tan\delta = \epsilon''/\epsilon'$$



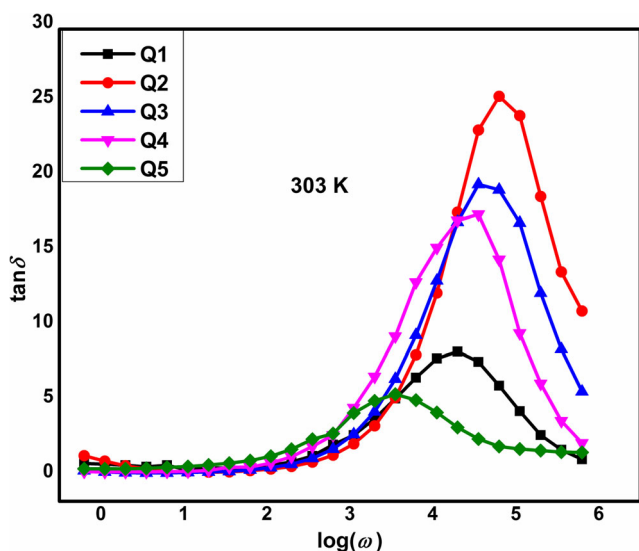


Fig. 10 Room temperature variation of  $\tan\delta$  as a function of  $\log\omega$  for the prepared samples

It has been observed that the  $\tan\delta$  increases with increasing frequency and reaches a maximum. Then, it decreases for further increasing the frequency. For maximum dielectric loss at a particular temperature, the absorption peak is described by the relation  $\omega\tau = 1$ , where  $\tau$  is the relaxation time and  $\omega$  is the angular frequency of the applied signal. It is clear that the temperature increase in the charge carriers has been thermally activated and the loss tangent peak shifts towards higher frequency. This indicates that the relaxation time decreases with increases of temperature.

**Transference ion number**

For energy storage application, the polymer electrolyte should be an ionic conductor. The DC polarization technique is used to evaluate the ion transference number in the polymer

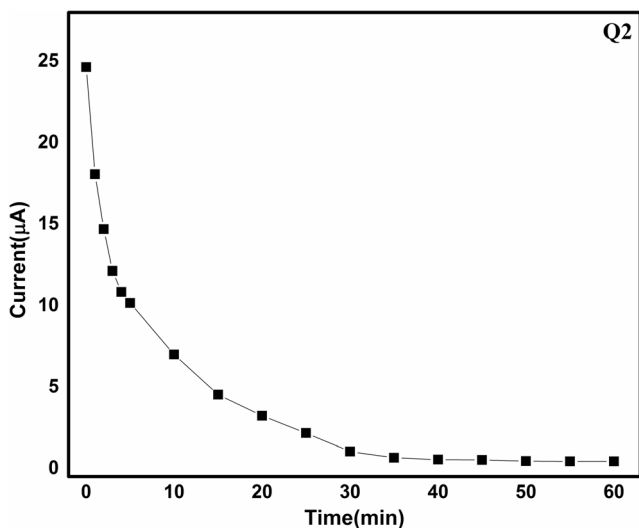


Fig. 11 DC polarization curve of the polymer electrolyte (Q2)

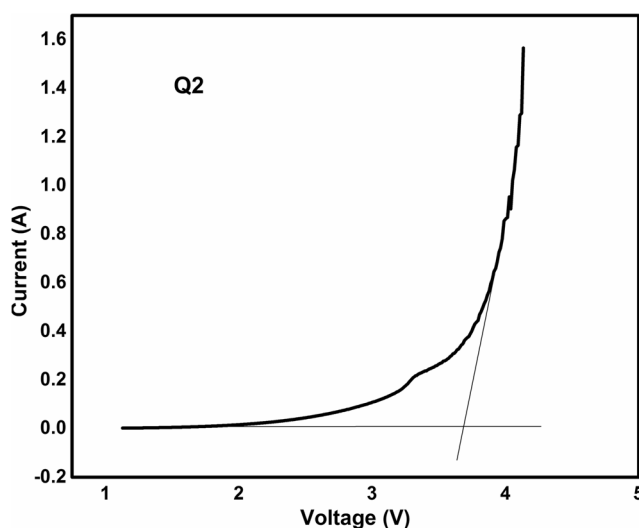


Fig. 12 Linear sweep voltammetry of Q2 film recorded at room temperature

electrolytes. The prepared polymer electrolyte was placed between the SS electrode, such as SS/PE/SS cell. In this method, the DC current was measured as a function of time on the application of fixed DC voltage across the cell. Then applying the 1.0 V, the current versus time plot was obtained. The obtained current vs time plot was shown in Fig. 11.

The transference ion number can be calculated from the dc polarization current vs time plot by using the following equation

$$t_{ion} = (I_i - I_f) / I_i$$

where  $t_{ion}$  is the ion transference number, and  $I_i$  and  $I_f$  are the initial and final current values of the cells. The ionic transference number for the polymer electrolyte (Q2) is obtained as

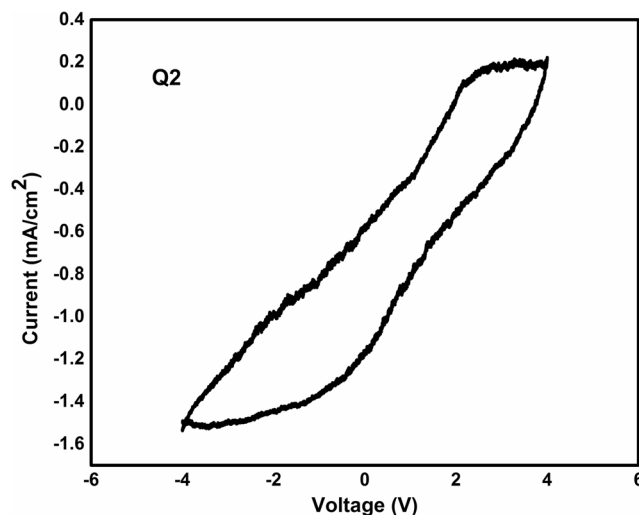


Fig. 13 Cyclic voltammograms (CVs) of Q2 film

0.98, respectively. This suggests that the charge transport in the polymer electrolyte is mainly due to the ions.

### Linear sweep voltammetry

The electrochemical stability of BPE is an important parameter for energy storage devices. The electrochemical stability of the maximum conducting BPE (Q2) film which has been measured using LSV and recorded on the SS/BPE/Mg cell was shown in Fig. 12. The voltage is swept from 0 V towards positive values with a scan rate of  $5 \text{ mV s}^{-1}$  until a large current is obtained at certain potential, which is due to the electrolyte decomposition at the inert electrode interface. The figure shows that the BPE (Q2) film is stable up to 3.68 V, which is a sufficient range for electrochemical applications especially for Mg batteries, and also compared to Pandey et al. [54], the value is high for blend system.

### Cyclic voltammetry

CV tests with Mg/GPE/Mg cells were carried out to check the  $\text{Mg}^{2+}$  ion conduction in the GPEs. The potential was swept from  $-4$  to  $4$  V at a rate of  $5 \text{ mV S}^{-1}$ . As can be shown in Fig. 13, the anodic peak appeared at about 2.45 V, implying that the polymer electrolyte has the voltage is more than 2 V. Also, the current peaks are distinctly observed. This reveals that the deposition and resolution of  $\text{Mg}^{2+}$  ion occur at the Mg/GPE interface.

From the analysis, the prepared polymer electrolyte has the electrochemical stability for the application of the rechargeable batteries, especially for the Mg ion battery application.

### Conclusion

A new  $\text{Mg}^{+}$  ion conducting PVdF-HFP-PVAc blend solid polymer electrolyte has been synthesized. The amorphous nature is confirmed by the XRD analysis. FTIR studies reveal the complex formation between the polymer matrix and salt. The AC conductivity value for all the prepared polymer electrolytes has been evaluated using impedance spectroscopy analysis. The high ionic conductivity has found to be  $3.85 \times 10^{-5} \text{ S cm}^{-1}$  at ambient temperature for Q2 sample. The activation energy obtained from conductivity data from  $E_a$  decreases with increasing ionic conductivity and vice versa. The electrochemical stability window, estimated from LSV, is found to be  $\sim 3.68$  V, which is sufficient for electrochemical applications. The CV suggests the existence of electrochemical equilibrium between the Mg metal and  $\text{Mg}^{+}$  ions in the BPE.

### References

1. Mohtadi R, Mizuno F (2014) Magnesium batteries: current state of the art, issues and future perspectives. *Beilstein J Nanotechnology* 5:1291–1311
2. Liu C, Zachary GN, Cao G (2016) *Mater Today*. 19(2):109–123. <https://doi.org/10.1016/j.mattod.2015.10.009>
3. Ha CJ, HyukYoon J, IlCho W, HoJang (2004) Electrochemical properties of  $\text{LiNi}_{0.8}\text{Co}_{0.2-x}\text{Al}_x\text{O}_2$ ? prepared by a sol–gel method. *J Power Sources* 136:132–138
4. Deng H, Nie P, Luo H, Zhang Y, Wang J, Zhang X (2014) Highly enhanced lithium storage capability of  $\text{LiNi}_{0.5}\text{Mn}_{1.5}\text{O}_4$ ? by coating with  $\text{Li}_2\text{TiO}_3$ ? for Li-ion batteries. *J Mater Chem A* 2(43):18256–18262
5. Aurbach D, Lu Z, Schechter A, Gofer Y, Gizbar H, Turgeman R, Cohen geman R, Cohen Y, Moshkovich M, Levi E (2000) Prototype systems for rechargeable magnesium batteries. *Nature* 407(6805):724–727
6. Pandey GP, Hashmi SA (2009) Experimental investigations of an ionic-liquid-based, magnesium ion conducting, polymer gel electrolyte. *J Power Sources* 187(2):627–634
7. Novak P, Imdhof R, Haas O (1999) Magnesium insertion electrodes for rechargeable nonaqueous batteries—a competitive alternative to lithium. *Electrochim Acta* 45(1-2):351–367
8. Wu N, Yang ZZ, Yao HR, Yin YX, Gu L, Guo YG (2015) Improving the electrochemical performance of  $\text{Li}_4\text{Ti}_5\text{O}_{12}$ ? electrode in a rechargeable Mg battery by lithium magnesium co-intercalation. *J Angew Chem Int Ed* 54(19):5757–5761
9. Tao ZL, Xu LN, Gou XL, Chen J, Yuan HI (2004)  $\text{TiS}_2$  nanotubes as the cathode materials of Mg ion batteries. *J Chem Comm* 18: 2080–2081
10. Kim J, Lee J, You J, Park MS, Hossain MSA, Yamauchi Y, Kim JH (2016) Conductive polymers for next generation energy storage systems, recent progress and new function. *MaterHoriz* 3:517–535
11. Gregory TD, Hoffman RJ, Winterton RC (1990) Nonaqueous electrochemistry of magnesium applications to energy storage. *J Electrochem Soc* 137(3):775–780
12. Kumar GG, Munichandriah N (2002) Poly(methylmethacrylate) magnesium triflate gel polymer electrolyte for solid state magnesium battery application. *J Electrochim Acta* 47(7):1013–1022
13. Yoshimoto N, Yakushiji S, Ishikawa M, Morita M (2003) Rechargeable magnesium batteries with polymeric gel electrolytes containing magnesium salts. *J. Electrochim Acta* 48(14-16):2317–2322
14. Polu AR, Kumar R (2012) Ionic conductivity and discharge characteristic studies of PVA-Mg  $(\text{CH}_3\text{COO})_2$ ? solid polymer electrolytes. *Int J Polymer Mater* 62:76–80
15. Polu AR, Kumar R (2014)  $\text{Mg}^{2+}$ -ion conducting poly(ethylene glycol)- $\text{TiO}_2$ ?composite polymer electrolytes for solid-state batteries. *Materials Express* 4:79–84
16. Ulaganathan M, Rajendran S (2010) Preparation and characterization of PVAc/P(VdF-HFP)-based polymer blend electrolytes. *Ionics* 16:515–521
17. Pandey GP, Agrawal RC, Hashmi SA (2011) Magnesium ion-conducting gel polymer electrolytes dispersed with fumed silica for rechargeable magnesium battery application. *J Solid State Electrochem* 15(10):2253–2264
18. Oh JS, Ko JM, Kim DW (2004) Preparation and characterization of gel polymer electrolytes for solid state magnesium batteries. *J Electrochim Acta* 50(2-3):903–906
19. Shakur MF, Ithnin R, Illias HA, Kadir MFZ (2013) Proton conducting polymer electrolyte based on plasticized chitosan-PEO and application in electrochemical devices. *Opt Mater* 35(10):1834–1841

20. Kalyanasundaram NT, Subramanian A, Lokesh KS, Muhammed Musthafa OT (2008) Effect of porosity on PVdF-HFP/PMMA based electrolyte. *J Materials Chem and Phy* 110:11–16
21. Basri NH, Mohamed NS (2009) Conductivity studies and dielectric behavior of PVdF-HFP/PVC LiClO<sub>4</sub> solid polymer electrolyte. *Solid State Sci Technol* 17:63–72
22. Rajendran S, Shanthi Bama V, Ramesh Prabhu M (2010) Effect of lithium salt concentration in PVAc/PMMA-based gel polymer electrolytes. *Ionics* 16(1):27–32
23. Lee H, Yanilmaz M, Toprakci O, Fu K, Zhang X (2014) PVdF-HFP/PVAc: a review of recent developments in membrane separators for rechargeable lithium-ion batteries. *J Energy Environ Sci* 7(12):3857–3886
24. JuHwangSoo Y, KyungJeong KSN, Manuel Stephan A (2007) Electrochemical studies on poly(vinylidene fluoride-hexafluoropropylene) membranes prepared by phase inversion method. *Eur Polym J* 43:65–71
25. Ulaganathan M, Rajendran S (2010) Effect of different salts on PVAc/PVdF-co-HFP based polymer blend electrolytes. *J Appl Polym Sci* 118:646–651
26. Kirankumar K, Ravi M, Pavani Y, Bhavani S, Sharma AK, VVR NR (2014) Investigations on PEO/PVP/NaBr complexed polymer blend electrolytes for electrochemical cell applications. *J Membr Sci* 454:200–211
27. Kim DW, Park JK, Rhee HW (1996) Conducting and thermal studies of solid polymer electrolytes prepared by poly(ethyleneoxide), poly(oligo[oxyethylene]oxysebacoyl) and lithium perchlorate. *Solid State Ionics* 83(1-2):49–56
28. Kim CH, Kim HT, Park JK, Moon SI, Yoon MS (1996) Preparation and ionic conductivities of the plasticized polymer electrolytes based on poly(methyl methacrylate-co-alkali metal methacrylate). *J polymer Sci: part B:Polymer Phys* 34(16):2709–2714
29. Sung HY, Wang YY, Wan CC (1998) Preparation and characterization of poly(vinyl chloride-co-vinyl acetate)-based gel electrolytes for Li-ion batteries. *J Electrochem Soc* 145(4):1207–1211
30. Rhoo HJ, Kim HT, Park JK, Hwang TS (1997) Ionic conduction in plasticized PVC/PMMA blend polymer electrolytes. *Electrochimica Acta* 42(10):1571–1579
31. Jian-HuaCao, Bao-KuZhu, You-YiXu (2006) Structure and ionic conductivity of porous polymer electrolytes based on PVDF-HFP copolymer membranes. *J Membr Sci* 281:446–453
32. Wiecek W, Florjanczyk Z, Stevens JR (1995) Proton conducting polymer gels based on a poly acrylamide matrix. *Electrochim Acta* 40:2327–2330
33. Shanmukaraj D, Wang GX, Murugan R, Liu HK (2008) Ionic conductivity and electrochemical stability of PMMA-PEO blend ceramic filler composites. *J Phys Chem Solids* 69(1):243–248
34. Prajapati GK, Roshan R, Gupta PN (2010) Effect of plasticizer on ionic transport and dielectric properties of PVA:H<sub>3</sub>PO<sub>4</sub>? proton conducting polymeric electrolyte. *J Phys and Chem of Solids* 71(12):1717–1723
35. Ulaganathan M, Rajendran S (2011) Novel Li-ion conduction on poly(vinyl acetate)-based hybrid polymer electrolytes with double plasticizers. *J Appl Electrochem* 41(1):83–88
36. Gebreyesus MA, Purushotham Y, Sivakumar J (2016) Preparation and characterization of lithium ion conducting polymer electrolytes based on a blend of poly(vinylidene fluoride-co-hexafluoropropylene) and poly(methyl methacrylate). *Heliyon* 2(7):e00134. <https://doi.org/10.1016/j.heliyon.2016.e00134>
37. Abbrent S, Plestil J, Hlavata D, Lindgren J, Tegenfeldt J, Wendsjo A (2001) Crystallinity and morphology of PVdF-HFP-based gel electrolytes. *Polymer* 42(4):1407–1416
38. Ataollahi N, Ahmad A, Hamzah H, Rahman MYA, Mohamed NS (2012) Preparation and characterization of PVDF-HFP/MG49 based polymer blend electrolyte. *Int J Electrochem Sci* 7:6693–6703
39. Tafur JP, Santos F, Fernández Romero AJ (2015) Influence of the ionic liquid on the gel polymer electrolytes properties. *Membranes* 5(4):752–771
40. Baskaran R, Selvasekarapandian S, Hirankumar G, Bhuvaneshwari MS (2004) Vibrational ac impedance and dielectric spectroscopic studies of poly(vinylacetate)-*N,N*-dimethylformamide-LiClO<sub>4</sub>? polymer gel electrolytes. *J Power Sources* 134(2):235–240
41. Baskaran R, Selvasekarapandian S, Kuwata N, Kawamura J, Hattori T (2007) Structure, thermal and transport properties of PVAc-LiClO<sub>4</sub>? solid polymer electrolytes. *J Phys and Chem Solids* 68(3):407–412
42. Arunkumar D, Selvasekarapandian S, Baskaran R, Savitha T, Nithya H (2012) Thermal vibrational and AC impedance studies on proton conducting polymer electrolytes based on poly(vinylacetate). *J Non crystal solids* 358:531–536
43. Ulaganathan M, Nithya R, Rajendran S, Raghu S (2012) Li-ion conduction on nanofiller incorporated PVdF-co-HFP based composite polymer blend electrolytes for flexible battery applications. *Solid State Ionics* 218:7–12
44. Michael MS, Jacob MME, Prabakaran SRS, Radhakrishna S (1997) Enhanced lithium ion transport in PEO-based solid polymer electrolytes employing a novel class of plasticizers. *Solid State Ionics* 98(3-4):167–174
45. Ulaganathan M, Chithra MM, Rajendran S (2013) Highly porous lithium ion conducting solvent free poly(vinylidene fluoride-co-hexafluoropropylene)/poly(ethyl methacrylate) based polymer blend electrolytes for Li battery applications. *J. Electrochim Acta* 93:230–235
46. Selvasekarapandian S, Baskaran R, Kamishima O, Kawamura J, Hattori T (2006) Laser Raman and FTIR studies on Li<sup>+</sup> interaction in PVAc-LiClO<sub>4</sub> polymer electrolytes. *J Spectrochim Acta part A* 65(5):1234–1240
47. Ulaganathan M, Sundar Pethaiah S, Rajendran S (2011) Li-ion conduction in PVAc based blend electrolytes for lithium battery applications. *J Mater Chem Phys* 129(1-2):471–476
48. Tsunemi K, Ohno H, Tsuchida A (1983) A mechanism of ionic conduction of poly(vinylidene fluoride)-lithium perchlorate hybrid films. *J. Electrochim Acta* 28(6):833–837
49. Park US, Hong YJ, Oh SM (1996) Fluorescence spectroscopy for local viscosity measurements in polyacrylonitrile (pan)-based polymer gel electrolytes. *J Electrochim Acta* 41(6):849–855
50. Missan HPS, Chu PP, Sekhon SS (2006) Ion conduction mechanism in non-aqueous polymer electrolytes based on oxalic acid: effect of plasticizer and polymer. *J Power Sources* 158(2):1472–1479
51. Polu AR, Kumar R (2013) Preparation and characterization of PVA based polymer electrolytes for electrochemical cell application. *Chinese J Polym Sci* 31(4):641–648
52. Tripathi SK, Jain A, Gupita A, Mishra M (2012) Electrical and electrochemical studies on magnesium ion-based polymer gel electrolytes. *J Solid State Electrochem* 16(5):1799–1806
53. Manjuladevi R, Thamilselvan M, Selvasekarapandian S, Mangalam R, Premalatha M, Monisha S (2017) Mg-ion conducting blend polymer electrolyte based on poly(vinyl alcohol)-poly(acrylonitrile) with magnesium perchlorate. *Solid State Ionics* 308:90–100
54. Pandey GP, Hashmi SA (2009) Experimental investigations of an ionic-liquid-based magnesium ion conducting polymer gel electrolytes. *J Power Sources* 187(2):627–634